CHEMISTRY
A EUROPEAN JOURNAL

DOI: 10.1002/chem.200701582

Polyhedral Structures with Three-, Four-, and Five Fold Symmetry in Metal-Centered Ten-Vertex Germanium Clusters

R. Bruce King,*[a] Ioan Silaghi-Dumitrescu,[b] and Matei-Maria Uţă[b]

Abstract: Studies using density functional theory (DFT) at the hybrid B3LYP level indicate that the relative energies of structures with three-fold, four-fold, and five-fold symmetry for centered 10-vertex bare germanium clusters of the general type $M@Ge_{10}^{z}$ depend on the central metal atom M and the skeletal electron count. For $M@Ge_{10}$ clusters with 20 skeletal electrons the DFT results agree with experimental data on the isoelectronic centered 10-vertex bare metal clusters. Thus the lowest energy structure for $Ni@Ge_{10}$, isoelectronic with the known $Ni@In_{10}^{10-}$, is a C_{3v} polyhedron derived from the tetracapped trigonal prism. However, $Zn@Ge_{10}^{2+}$ is isoelectronic with the known cluster $Zn@In_{10}^{8-}$, which has the lowest energy structure, a D_{4d} bicapped square antiprism. For the clusters $Ni@Ge_{10}^{2-}$, $Cu@Ge_{10}^{-}$, and $Zn@Ge_{10}$ that have 22 skeletal electrons the lowest energy structures are the D_{4d} bicapped square antiprism predicted by the Wade–Mingos rules. For the clusters $Ni@Ge_{10}^{4-}$, $Cu@Ge_{10}^{3-}$, and $Zn@Ge_{10}^{2-}$ that have 24 skeletal electrons the lowest energy structures are C_{3v} polyhedra with 10 triangular faces and 3 quadrilateral faces derived from a tetracapped trigonal prism by extreme lengthening of the edges of the capped triangular face of the underlying trigonal prism. For the clusters $Cu@Ge_{10}^{5-}$ and $Zn@Ge_{10}^{4-}$ that have 26 skeletal electrons the lowest energy structures are the D_{5d} pentagonal antiprisms predicted by the Wade–Mingos rules and the C_{3v} tetracapped trigonal prism as a somewhat higher energy structure. However, for the isoelectronic $Ni@Ge_{10}^{6-}$ the relative energies of these two structure types are reversed so that the C_{3v} tetracapped trigonal prism becomes the global minimum. The effects of electron count on the geometries of the D_{5d} pentagonal prism and D_{4d} bicapped square antiprism centered metal cluster structures are consistent with the bonding/antibonding characteristics of the corresponding HOMO and LUMO frontier molecular orbitals.

Keywords: cluster compounds · copper · endohedral clusters · germanium · nickel · Wade–Mingos rules · zinc

Introduction

Ten-vertex Zintl cluster ions are of interest because of their ability to accommodate interstitial transition metal and post-transition metal atoms.[1,2] However, the centered ten-vertex polyhedra in such Zintl cluster ions are known to have different shapes depending on the central metal atom and the skeletal electron count. Thus for the ions $M@In_{10}^{10-}$ (M = Ni, Pd, Pt) found in the intermetallics $K_{10}In_{10}M$ the In_{10} polyhedron is a C_{3v} tetracapped trigonal prism (Figure 1).[3] However, for the isoelectronic ion $Zn@In_{10}^{8-}$ found in the intermetallic $K_8In_{10}Zn$ the In_{10} polyhedron is a D_{4d} bicapped square antiprism (Figure 1).[4] Furthermore the

[a] Prof. R. B. King
Department of Chemistry, University of Georgia
Athens, Georgia, 30602 (USA)
Fax: (+1)706-542-9454
E-mail: rbking@chem.uga.edu

[b] Prof. I. Silaghi-Dumitrescu, Dr. M.-M. Uţă
Faculty of Chemistry and Chemical Engineering
Babeş-Bolyai University, Cluj-Napoca (Romania)

Supporting information for this article is available on the WWW under http://www.chemeurj.org/ or from the author. The optimized structures of $M@Ge_{10}^{z}$ can be found in Table S1 with their energies and geometries.

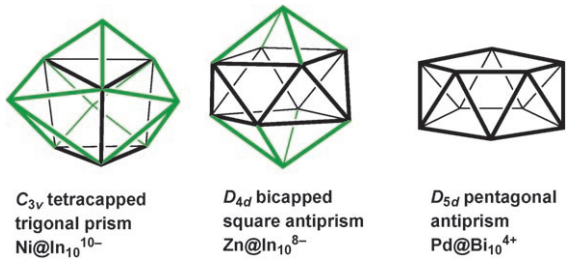

Figure 1. Ten-vertex polyhedra exhibiting three-, four-, and five-fold symmetry found in centered bare post-transition metal clusters. For clarity the caps are depicted in green and the underlying polyhedra in black.

Bi_{10} polyhedron in the 26 skeletal electron $Pd@Bi_{10}^{4+}$ found in $Bi_{14}PdBr_{16}$ ($=[Pd@Bi_{10}][BiBr_4]_4$)[5] is different from either of these polyhedra, but instead is a D_{5d} pentagonal antiprism (Figure 1). Thus polyhedra of three-, four-, and five-fold symmetry are found in metal-centered ten-vertex post-transition metal clusters.

The objective of the research is to study the effects of interstitial atoms and electron count on cluster geometry using density functional theory (DFT) methods. Germanium clusters with interstitial Ni, Cu, and Zn atoms were chosen as tractable systems with minimum charges, but having vertices isolobal to the Group 13 to 15 metal atom vertices found in the known ten-atom inorganic clusters with interstitial atoms. The range of charges on $M@Ge_{10}^{z}$ chosen for this work spans the 20 skeletal electrons found in the known derivatives[3,4] $Ni@In_{10}^{10-}$ and $Zn@In_{10}^{8-}$ to the 26 skeletal electrons required for an *arachno* ten-vertex cluster ($26=2n+6$ for $n=10$) such as the known[5] $Pd@Bi_{10}^{4+}$. Note that in counting the skeletal electrons in these systems the filled d^{10} shell of the interstitial atom is formally considered to be unavailable for skeletal bonding so that interstitial Ni, Cu, and Zn atoms contribute 0, 1, and 2 skeletal electrons, respectively. The choice of germanium as the vertex atom for this study of the centered ten-vertex clusters minimizes the maximum charge required for the range of skeletal electrons of interest thereby facilitating the calculations. Although no ten-vertex germanium clusters are known experimentally, the related ten-vertex clusters Pb_{10}^{2-} (ref. [6]) and $Ni@Pb_{10}$ (ref. [7]) are known and contain the heavier Group 14 element lead.

Isoelectronic and isolobal relationships provide analogies of our DFT results on $M@Ge_{10}^{z}$ clusters (M=Ni, Cu, Zn) to experimentally known related metal centered clusters with group 13 vertices (indium) or group 15 vertices (bismuth).

Computational Methods

Geometry optimizations were carried out at the hybrid DFT B3LYP level[8,9,10,11] with the 6-31G(d) (valence) double zeta quality basis functions extended by adding one set of polarization (d) functions. The Gaussian 98 package of programs[12] was used in which the fine grid (75,302) is the default for numerically evaluating the integrals and the tight (10^{-8}) Hartree stands as default for the self-consistent field convergence. Computations were carried out using four initial geometries including ten-vertex polyhedra with three-fold, four-fold, and five-fold symmetry (Figure 2). The symmetries were maintained during the geometry optimization processes. In addition, symmetry breaking by using modes defined by imaginary vibrational frequencies was used to determine optimized structures with minimum energies. Vibrational analyses show that all of the final optimized structures discussed in this paper are genuine minima at the B3LYP/6-31G(d) level without any significant imaginary frequencies ($N_{imag}=0$). In a few cases the calculations ended with acceptable small imaginary frequencies[13] and these values are indicated in the corresponding figures.

The optimized structures found for the $M@Ge_{10}^{z}$ clusters are labeled by the number of skeletal electrons, the order of the principal rotation axis, and the central metal atom with significant distortions from ideal symmetry indicated by **D**, for example **24-4D(Cu)**. Thus the C_{3v} isomer of neutral $Ni@Ge_{10}$ is labeled **20–3(Ni)**. Additional details of all of the optimized structures, including all interatomic distances and the initial geometries leading to a given optimized structure, are provided in the Supporting Information. In assigning polyhedra to the optimized structures, the Ge–Ge distances less than ≈3.2 Å were normally considered as polyhedral edges; significant exceptions are discussed in the text.

Metal–cluster molecular orbital interaction diagrams have been drawn with the aid of the ADF-2007.01 package of programs.[14]

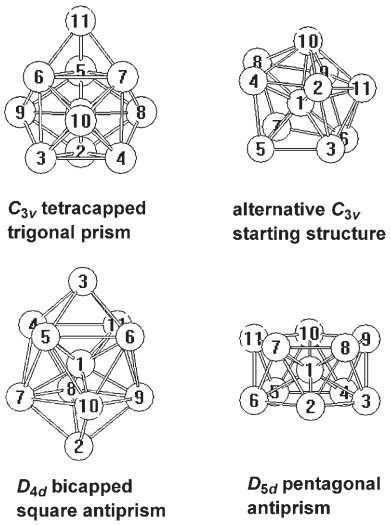

Figure 2. The starting structures used for the $M@Ge_{10}$ optimizations.

Results

Structures with 20 skeletal electrons: The structures that have 20 skeletal electrons are of particular interest because the isoelectronic $Ni@In_{10}^{10-}$ and $Zn@In_{10}^{8-}$ are found experimentally to have different structures, namely the C_{3v} tetracapped trigonal prism[3] for $Ni@In_{10}^{10-}$ and the D_{4d} bicapped square antiprism[4] for $Zn@In_{10}^{8-}$. Our calculations on the isoelectronic $Ni@Ge_{10}$ and $Zn@Ge_{10}^{2+}$ are consistent with this experimental observation (Figure 3). For all three interstitial metals the C_{3v} and D_{4d} isomers (**20–3** and **20–4**, respectively) are seen to be very close to each other in energy with a maximum of 4.6 kcal mol^{-1} difference for the nickel derivatives. Furthermore, the D_{4d} isomer is increasingly favored in going from Ni to Zn so that for $Ni@Ge_{10}$ and

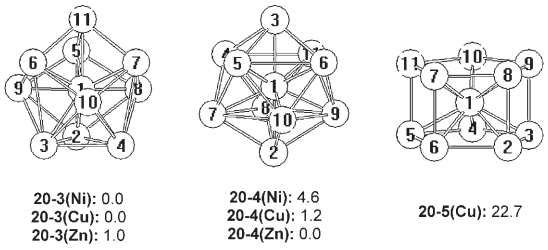

Figure 3. The three types of optimized structures for the 20 skeletal electron systems $Ni@Ge_{10}$, $Cu@Ge_{10}^{+}$, and $Zn@Ge_{10}^{2+}$ with the relative energies indicated in kcal mol^{-1}.

$Cu@Ge_{10}^{+}$ the C_{3v} isomers are the global minima whereas for $Zn@Ge_{10}^{2+}$ the relative energies are interchanged so that the D_{4d} isomer is the global minimum. A D_{5h} pentagonal prismatic isomer **20–5(Cu)** is also found for $Cu@Ge_{10}^{+}$ at 22.7 kcal mol^{-1} above the global minimum **20–3(Cu)** (Figure 3). No D_{5h} or D_{5d} isomer was found for the Ni derivative $Ni@Ge_{10}$.

Structures with 22 skeletal electrons: The D_{4d} bicapped square antiprismatic structure dominates for the $M@Ge_{10}$ derivatives with 22 skeletal electrons (Figure 4). This is consistent with the Wade–Mingos rules[15,16,17,18] predicting this most spherical deltahedron for a *closo* 22 skeletal electron system as exemplified by the well-known $B_{10}H_{10}^{2-}$ in borane chemistry.[19] In addition the bicapped square antiprismatic cluster structure is found for the closely related lead cluster $Ni@Pb_{10}^{2-}$, which has been isolated and characterized by X-ray diffraction.[7] Attempted optimization from a D_{5h} pentagonal antiprism starting point (Figure 2) for these systems with 22 skeletal electrons leads to distorted pentagonal prismatic rather than antiprismatic stationary states for $Cu@Ge_{10}^{-}$ and $Zn@Ge_{10}$ at 12.7 and 22.7 kcal mol^{-1}, respectively, above the **22–4** D_{4d} global minima, apparently by rotation of one pentagonal face relative to the other one in the original antiprism. However, a true D_{5d} pentagonal antiprismatic stationary state is obtained for $Ni@Ge_{10}^{2-}$, but at the relatively high energy of 38.0 kcal mol^{-1} above the **22–4** global minimum (Figure 4). In addition, C_{3v} tetracapped trigonal prism stationary states are found for all three derivatives, but at 14 to 28 kcal mol^{-1} above the global minima (Figure 4).

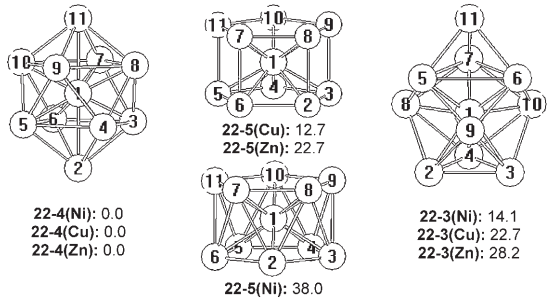

Figure 4. The optimized structures for the 22 skeletal electron systems $Ni@Ge_{10}^{2-}$, $Cu@Ge_{10}^{-}$, and $Zn@Ge_{10}$ with the relative energies indicated in kcal mol^{-1}.

Structures with 24 skeletal electrons: The Wade–Mingos rules[15,16,17,18] predict a polyhedron with one non-triangular face for a ten-vertex polyhedral cluster with a 24 skeletal electron count. For example, the *nido* borane $B_{10}H_{14}$ has a polyhedral structure with one large hexagonal face.[20] However, the lowest energy structure for all three of the 24 skeletal electron systems $Ni@Ge_{10}^{4-}$, $Cu@Ge_{10}^{3-}$, and $Zn@Ge_{10}^{2-}$ is a C_{3v} polyhedron with three quadrilateral faces (Figure 5) in contradiction to the Wade–Mingos rules.[15,16,17,18]

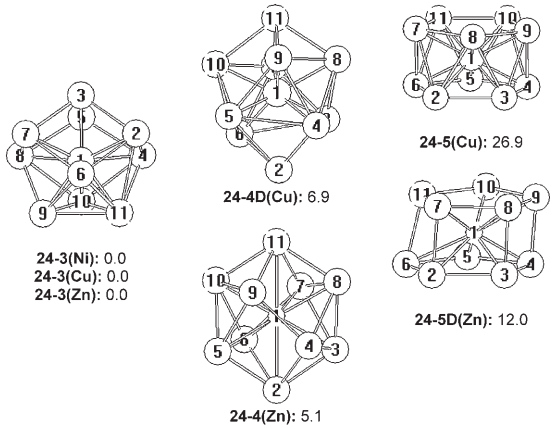

Figure 5. The optimized structures for the 24-skeletal electron systems $Ni@Ge_{10}^{4-}$, $Cu@Ge_{10}^{3-}$, and $Zn@Ge_{10}^{2-}$ with the relative energies indicated in kcal mol^{-1}.

No other structures were found for $Ni@Ge_{10}^{4-}$. For the copper derivative $Cu@Ge_{10}^{3-}$ optimization of the D_{4d} bicapped square antiprism led to a highly distorted structure **24–4D(Cu)** at 6.9 kcal mol^{-1} above the global minimum **24–3(Cu)** (Figure 5). For the isoelectronic zinc derivative $Zn@Ge_{10}^{2-}$ an analogous optimization from the D_{4d} bicapped square antiprism retained the general shape, but resulted in significant elongation to give structure **24–4(Zn)** at 5.1 kcal mol^{-1} above the global minimum **24–3(Zn).**

Still higher energy structures are found for $Cu@Ge_{10}^{3-}$ and $Zn@Ge_{10}^{2-}$ starting with the D_{5d} pentagonal antiprism (Figure 5). For the copper derivative the five-fold symmetry is retained to give structure **24–5(Cu)** at 26.9 kcal mol^{-1} above the global minimum **24–3(Cu)**. However, an analogous optimization of the zinc derivative leads to considerable distortion of the pentagonal antiprism to give the "Leaning Tower of Pisa" distorted pentagonal prismatic structure **24–5D(Zn)** at 12.0 kcal mol^{-1} above the global minimum **24–3(Zn)**.

Structures with 26 skeletal electrons: The Wade–Mingos rules[15,16,17,18] suggest an *arachno* structure with two open (non-triangular) faces for a 10-vertex cluster and $2n+6$ skeletal electrons. The most obvious possibility is the pentagonal antiprism found experimentally[5] in the 26 skeletal electron system $Pd@Bi_{10}^{4+}$ in $[Pd@Bi_{10}][BiCl_4]_4$. The global minima for the isoelectronic $Cu@Ge_{10}^{5-}$ and $Zn@Ge_{10}^{4-}$ are also the D_{5d} pentagonal antiprisms **26–5(Cu)** and **26–5(Zn)**. However, for the isoelectronic $Ni@Ge_{10}^{6-}$, which would be a more direct analogue of the known $Pd@Bi_{10}^{4+}$, the analogous pentagonal antiprismatic structure **26–5(Ni)** lies 17.6 kcal mol^{-1} above the global minimum **26–3(Ni)**.

The global minimum for $Ni@Ge_{10}^{6-}$ is a C_{3v} structure **26–3(Ni)**, which has similar topology to the C_{3v} structure of the 20 skeletal electron $Ni@Ge_{10}$, but elongated significantly (Figure 6). The analogous C_{3v} structure for the isoelectronic

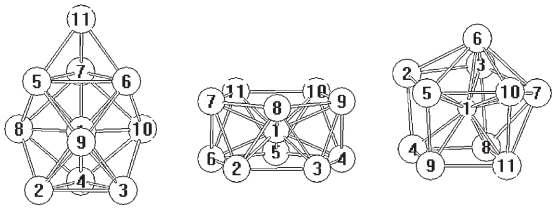

Figure 6. The optimized structures for the 26 skeletal electron systems $Ni@Ge_{10}^{6-}$, $Cu@Ge_{10}^{5-}$, and $Zn@Ge_{10}^{4-}$ with the relative energies indicated in kcal mol^{-1}.

$Cu@Ge_{10}^{5-}$ isomer, namely **26–3(Cu)**, lies only 1.0 kcal mol^{-1} above the pentagonal antiprismatic global minimum **26–5(Cu).** However, the corresponding $Zn@Ge_{10}^{4-}$ isomer **26–3(Zn)** lies 16.6 kcal mol^{-1} above the D_{5d} global minimum **26–1(Zn)**. In addition, an even higher energy distorted $Zn@Ge_{10}^{4-}$ isomer **26–2(Zn)** at 18.3 kcal mol^{-1} above **26–2(Zn)** is found starting from the D_{4d} bicapped square antiprism.

Discussion

Pentagonal antiprismatic structures—structures with a C_5 axis: The pentagonal antiprismatic structure of fivefold symmetry (D_{5d}) predicted by the Wade–Mingos rules[15,16,17,18] for ten-vertex systems with 26 skeletal electrons is found experimentally[5] in $Pd@Bi_{10}^{4+}$ and is predicted here by DFT for the isoelectronic systems $Ni@Ge_{10}^{6-}$, $Cu@Ge_{10}^{5-}$, and $Zn@Ge_{10}^{4-}$. In our previous DFT studies[21] a similar pentagonal antiprismatic structure was also found for the empty cluster Ge_{10}^{6-} with 26 skeletal electrons. For other skeletal electron counts an undistorted pentagonal antiprismatic structure is found only for $Ni@Ge_{10}^{2-}$ with 22 skeletal electrons. Attempts to optimize pentagonal antiprismatic structures for the isoelectronic $Cu@Ge_{10}^{-}$ and $Zn@Ge_{10}$, also with 22 skeletal electrons, led to rotation of one pentagonal face relative to the other to give pentagonal prismatic structures (Figure 4).

A pentagonal antiprism of D_{5d} symmetry has two different edge lengths, namely the lengths of the ten equivalent sides of the two pentagonal faces (the "horizontal" edge length, h) and those of the ten edges connecting a vertex of one pentagonal face with the other pentagonal face (the "vertical" edge length, v). The ratio v/h between these two edge lengths can be used to characterize the amount of elongation of the pentagonal antiprism. High v/h ratios correspond to elongated (prolate) structures and relatively low v/h ratios indicate compressed (oblate) structures.

Table 1 summarizes the v/h ratios and related geometric parameters for various computed pentagonal antiprismatic structures as well as the experimental structure[5] for $Pd@Bi_{10}^{4+}$. For all of the systems with 26 skeletal electrons studied the v/h ratio falls in the narrow range from 0.93 for

Table 1. Dimensions of pentagonal antiprismatic metal clusters [Å].

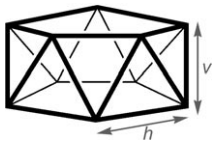

Cluster	v	h	v/h	$M@E_{10}$ distance
26 skeletal electrons				
Ge_{10}^{6-} (empty)	2.67	2.74	0.97	–
$Ni@Ge_{10}^{6-}$	2.64	2.84	0.93	2.65
$Cu@Ge_{10}^{5-}$	2.66	2.81	0.95	2.64
$Zn@Ge_{10}^{4-}$	2.68	2.79	0.96	2.63
$Pd@Bi_{10}^{4+}$ (exptl)[a]	3.15	3.16	1.00	3.00
22 skeletal electrons				
$Ni@Ge_{10}^{2-}$	2.83	2.53	1.12	2.49

[a] Ref. [5]

$Ni@Ge_{10}^{6-}$ to the experimental value[5] of 1.00 for $Pd@Bi_{10}^{4+}$. The presence of the interstitial metal atom is seen to have relatively little effect on the shape on the pentagonal antiprism since the v/h ratio of 0.97 for the empty Ge_{10}^{6-} pentagonal antiprism falls in the middle of this range. For the single system with 22 skeletal electrons with pentagonal antiprism geometry found in this work, namely $Ni@Ge_{10}^{2-}$, a significantly higher v/h ratio of 1.12 was found (Table 1) indicating significant elongation of the pentagonal antiprism upon removal of four skeletal electrons from $Ni@Ge_{10}^{6-}$.

The geometries of the D_{5d} pentagonal antiprismatic $M@Ge_{10}$ clusters can be rationalized by consideration of the frontier molecular orbitals. In this connection both the HOMO and LUMO of $Ni@Ge_{10}^{2-}$ with 22 skeletal electrons are doubly degenerate, namely e_{2g} and e_{1g}, respectively (Figure 7). This implies that similar D_{5d} pentagonal anti-

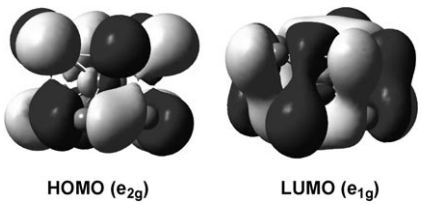

Figure 7. The frontier orbitals of the pentagonal antiprism cluster $Ni@Ge_{10}^{2-}$ with 22 skeletal electrons. Both the HOMO and LUMO depicted in this figures are one representative of a pair of degenerate e_{2g} and e_{1g} orbitals, respectively.

prism centered 10-vertex metal clusters with either 20 or 24 skeletal electrons will have open shells, namely a half-filled HOMO or a half-filled LUMO, respectively, and thus should either be triplets or undergo Jahn–Teller distortion from ideal D_{5d} symmetry.

Consider also the four-electron reduction of the D_{5d} pentagonal antiprismatic $Ni@Ge_{10}^{2-}$ to $Ni@Ge_{10}^{6-}$ thereby increasing the number of skeletal electrons from 22 to 26. The extra four electrons fill both orbitals of the e_{1g} LUMO pair, which is bonding between the two pentagonal faces of the antiprism in the direction of the C_5 axis (Figure 7). There-

fore, four-electron reduction of pentagonal antiprismatic $Ni@Ge_{10}^{2-}$ to $Ni@Ge_{10}^{6-}$ should result in compression of the antiprism to a more oblate structure. This is consistent with the decrease of the v/h ratio from 1.12 in $Ni@Ge_{10}^{-2}$ to 0.93 in $Ni@Ge_{10}^{6-}$ (Table 1).

Bicapped square antiprismatic structures—structures with a C_4 axis: The bicapped square antiprism structure with fourfold symmetry (D_{4d}) is found experimentally[4] in the 20 skeletal electron centered cluster $Zn@In_{10}^{8-}$ as well as in a number of 22 skeletal electron structures including $B_{10}H_{10}^{2-}$ and its numerous substitution products and the phosphorus-centered metal carbonyl cluster[22] $P@Co_{10}(CO)_{22}^{3-}$. Our DFT calculations find the bicapped square antiprism to be the global minima for the 22 skeletal electron systems $Ni@Ge_{10}^{2-}$, $Cu@Ge_{10}^{-}$, and $Zn@Ge_{10}$ in accord with the Wade–Mingos rules.[15,16,17,18] In addition, bicapped square antiprismatic structures are found for the 20 skeletal electron systems $Ni@Ge_{10}$, $Cu@Ge_{10}^{+}$, and $Zn@Ge_{10}^{2+}$, albeit not as global minima. A distorted bicapped square antiprismatic structure is also found for the 24-skeletal electron $Zn@Ge_{10}^{2+}$.

A bicapped square antiprism of D_{4d} symmetry has the following three different edge lengths (Table 1):

1) The lengths of the eight equivalent sides of the two square faces of the underlying square antiprism (the "horizontal" edge length, h).
2) The lengths of the eight edges connected a vertex of one square face of the underlying square antiprism with the other square face (the "vertical" edge length, v).
3) The eight equivalent edges connecting vertices of the square faces of the underlying square antiprism with one of the two caps (the "capping" edge length, c).

As is the case with the pentagonal antiprism discussed above, the elongation of the bicapped square antiprism can be measured by the v/h ratio as given in Table 1. Also the antipodal distance between the two caps of the bicapped square antiprism (a) is a good measure of the elongation or compression. However, this distance, as it is obviously not a bonding distance, is not easy to extract from published structural data. Also note that the designations here of h, v, c, and a for the horizontal, vertical, and capping edge lengths and the antipodal distances, respectively, correspond to the distances designated as h, d, c, and v in a previous paper.[21] This change was made for consistency with the pentagonal antiprismatic structures discussed above.

Consider first the bicapped square antiprismatic structures with 22 skeletal electrons since they are the global minima for both the empty and metal-centered structures in accord with the Wade–Mingos rules.[15,16,17,18] The shape of the bicapped square antiprism is seen to change very little upon incorporation of a metal atom in the center as indicated by the very small change in the v/h ratio from 0.90 in the empty Ge_{10}^{2-} cluster to 0.88 in the filled $M@Ge_{10}$ clusters (Table 2). Furthermore, the antipodal distance $a = 5.33$ Å in the empty Ge_{10}^{2-} cluster is within the 5.29–5.41 Å range found in the filled $M@Ge_{10}$ clusters. However, the size of the Ge_{10} cluster is seen to expand when a metal atom is placed as indicated by expansions of the v distances from 2.54 Å to 2.66–2.73 Å, the h distances from 2.82 Å to 3.03–3.09 Å, and the c distances from 2.59 Å to 2.67–2.73 Å upon going from the empty cluster to the filled $M@Ge_{10}$ clusters. In the bicapped square antiprismatic $M@Ge_{10}$ clusters with 22 skeletal electrons the distances from the central metal atom M to the two capping Ge vertices fall in the range 2.65–2.70 Å, which is approximately 0.27 Å longer than the distances in the range 2.38–2.43 Å from M to the remaining eight Ge vertices, namely those of the underlying square antiprism (Table 2). This suggests stronger bonding of the central metal atom to the vertices of the underlying square antiprism than to the remaining two capping vertices. This is consistent with the fact that from the sp^3d^5 manifold of the central metal atom a set of eight sp^3d^4 orbitals can be generated pointing to the vertices of a square antiprism. The metal d orbital not used for the square antiprismatic hybrid orbitals is the d_{z^2} orbital, which is suitably situated to form longer three-center bonds with the two antipodal vertex atoms.

The complete set of three centered bicapped square antiprismatic $M@Ge_{10}$ derivatives with 20 skeletal electrons is also found in this work, although not as global minima. The deltahedra in the derivatives with 20 skeletal electrons are significantly compressed over those in the derivatives with 22 skeletal electrons as indicated by a reduction of the antipodal distance $a = 5.29$–5.41 Å in the 22-skeletal electron derivatives $Ni@Ge_{10}^{2-}$, $Cu@Ge_{10}^{-}$, and $Zn@Ge_{10}$ to 4.73–

Table 2. Dimensions of bicapped square antiprismatic metal clusters [Å].

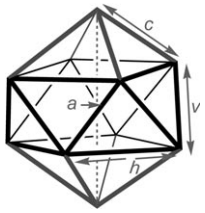

Cluster	v	h	c	a	v/h	$M@E_{10}$ distances
24 skeletal electrons						
Ge_{10}^{4-} (triplet)	2.63	2.76	2.72	5.96	0.95	–
$Zn@Ge_{10}^{2-}$	2.81	3.13	2.71	5.31	0.90	2.66(2),2.54(4), 2.43(4)
22 skeletal electrons						
Ge_{10}^{2-}	2.54	2.82	2.59	5.33	0.90	–
$Ni@Ge_{10}^{2-}$	2.66	3.03	2.67	5.29	0.88	2.65(2), 2.38(8)
$Cu@Ge_{10}^{-}$	2.69	3.05	2.69	5.36	0.88	2.68(2), 2.40(8)
$Zn@Ge_{10}$	2.73	3.09	2.73	5.41	0.88	2.70(2), 2.43(8)
20 skeletal electrons						
Ge_{10} (triplet)	2.60	2.76	2.61	5.61	0.94	–
$Ni@Ge_{10}$	2.61	3.13	2.60	4.73	0.83	2.37(2), 2.43(8)
$Cu@Ge_{10}^{+}$	2.67	3.16	2.62	4.78	0.84	2.39(2), 2.46(8)
$Zn@Ge_{10}^{2+}$	2.74	3.22	2.66	4.87	0.85	2.44(2), 2.51(8)
$Zn@In_{10}^{8-}$ (exptl)[a]	3.10	3.64	3.04	5.63	0.85	2.82(2), 2.84(8)

[a] Ref. [4].

4.87 Å in the 20-skeletal electron derivatives Ni@Ge_{10}, Cu@Ge_{10}^{+}, and Zn@Ge_{10}^{2+} (Table 2). As a result of this compression the two distances of the central metal atom to the capping vertices (2.37–2.44 Å) are slightly smaller than eight distances of the central metal atom to the vertices of the underlying square antiprism (2.43–2.51 Å) so that the interactions of the central metal atoms with all ten vertices of the bicapped square antiprism are nearly equal.

One example of a centered bicapped square antiprismatic derivative with 24 skeletal electrons is found, namely the zinc derivative Zn@Ge_{10}^{2-}. In this structure the ideal D_{4d} structure of the bicapped square antiprism is distorted to a lower symmetry structure (averages of the *h*, *v*, and *c* distances are listed in Table 2). Other than this distortion the bicapped square antiprism in the 24 skeletal electron Zn@Ge_{10}^{2-} is fairly similar to that in its 22 skeletal electron analogue Zn@Ge_{10}, as indicated by an antipodal distance of 5.31 Å versus 5.41 Å and *v*, *h*, and *c* edge lengths of 2.81, 3.13, and 2.71 Å versus 2.73, 3.09, and 2.73 Å, respectively.

The geometries of the D_{4d} bicapped square antiprismatic M@Ge_{10} clusters can be rationalized by consideration of the frontier molecular orbitals. Thus for the 22 skeletal electron cluster Ni@Ge_{10}^{2-} the HOMO is antibonding in the direction of the C_4 axis (Figure 8). Removal of the two HOMO

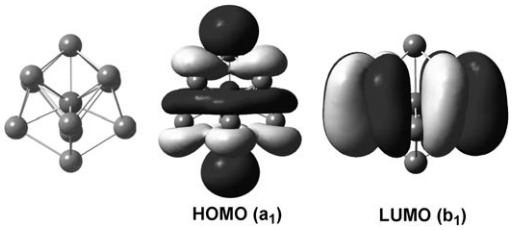

Figure 8. The frontier orbitals of the D_{4d} bicapped square antiprism cluster Ni@Ge_{10}^{2-} with 22 skeletal electrons relative to the indicated orientation of the bicapped square antiprism.

electrons in oxidizing Ni@Ge_{10}^{2-} to Ni@Ge_{10} should increase the bonding in the direction of the C_4 axis thereby decreasing the antipodal distance *a*. This is consistent with our calculations (Table 2) indicating that *a* decreases from 5.29–5.41 Å in the bicapped square antiprismatic clusters with 22 skeletal electrons to 4.73–4.78 Å in such clusters with only 20 skeletal electrons.

Consider now the two-electron reduction of Ni@Ge_{10}^{2-} to the centered cluster Ni@Ge_{10}^{4-} with 24 skeletal electrons. The added two electrons go into a LUMO, which has a node along the C_4 axis of the bicapped square antiprism and thus is non-bonding along the C_4 axis (Figure 8). This suggests that reduction from Ni@Ge_{10}^{2-} to Ni@Ge_{10}^{4-} should lead to relatively little change in the antipodal distance *a*. This again is consistent with our calculations indicating that the *a* of 5.31 Å for the cluster Zn@Ge_{10}^{2-} with 24 skeletal electrons is relatively close to the *a* of 5.41 Å for the corresponding cluster with 22 skeletal electrons.

Structures with a C_3 axis derived from the tetracapped trigonal prism: Structures derived from the tetracapped trigonal prism with C_{3v} symmetry are found for the metal-centered ten-vertex clusters with all even skeletal electron counts from 26 to 20. Furthermore, the clusters M@In_{10}^{10-} (M = Ni, Pd, Pt) with 20 skeletal electrons are known experimentally in the intermetallics $K_{10}In_{10}M$ and have been characterized by X-ray diffraction.[3]

The 24 edges of the tetracapped trigonal prism can be partitioned into the following six types:

1) The three vertical edges of the underlying trigonal prism of length *v*.
2) The three edges of the capped triangular face of the underlying trigonal prism of length h_c.
3) The three edges of the uncapped triangular face of the underlying trigonal prism of length h_u.
4) The six edges connecting the caps of the quadrilateral faces of the underlying trigonal prism to the vertices of its uncapped triangular face.
5) The six edges connecting the caps of the quadrilateral faces of the underlying trigonal prism to the vertices of its capped triangular face.
6) The three edges from the unique vertex capping a triangular face of the underlying trigonal prism and lying on the C_3 axis.

The lengths of the nine edges of the underlying trigonal prism, designated as *v*, h_c, and h_u as indicated above, can be used to characterize the shapes of the C_{3v} polyhedra derived from the tetracapped trigonal prism in cluster structures with various electron counts as summarized in Table 3. In many cases the cap at one end of the underlying trigonal prism makes the lengths h_c and h_u very different so that their difference $h_c - h_u = \Delta h$ can be used to measure the distortion of the underlying trigonal prism from its original D_{3h} symmetry to the C_{3v} structure with a cap at one end. The vertex capping the triangular face of the underlying trigonal prism is conveniently called the *axial* vertex in these structures since it is the only one of the ten vertices on the C_3 axis. In addition the ratio $v/\bar{h}$ can be used to measure the elongation of the tetracapped trigonal prism where $\bar{h}$ is the mean of h_c and h_u, i.e., $(h_c + h_u)/2$.

The shapes of the C_{3v} polyhedra found in the metal-centered ten-vertex clusters, as indicated by the $v/\bar{h}$ ratio and Δh of the underlying trigonal prism, is seen to depend drastically on the skeletal electron count. Consider first the systems with 20 skeletal electrons corresponding to the known[3] M@In_{10}^{10-} (M = Ni, Pd, Pt). In the C_{3v} polyhedron of the empty Ge_{10} cluster optimized in our previous work[21] the $v/\bar{h}$ ratio is 0.94 and Δh is 0.33 Å. Insertion of a metal in the center of this polyhedron moves the axial vertex closer to the center so that all ten M–Ge distances are within 2.6 Å. This distortion lengthens drastically the size of the capped triangular face of the underlying trigonal prism so that Δh increases from 0.33 Å in the empty Ge_{10} polyhedron to 0.84–0.92 Å depending on the central metal atom. Com-

Table 3. Dimensions of bicapped square antiprismatic metal clusters [Å].

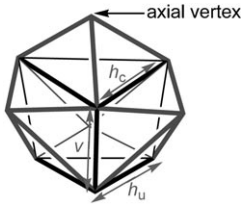

Cluster	v	h_c	h_u	Δh	$\bar{h}$	$v/\bar{h}$	$M@E_{10}$ distances
26 skeletal electrons							
Ge_{10}^{6-}	3.65	2.66	2.77	−0.11	2.71	1.35	–
$Ni@Ge_{10}^{6-}$	3.68	3.06	2.76	0.30	2.91	1.26	2.36(3),2.50(6),3.81(1)
$Cu@Ge_{10}^{5-}$	3.71	2.96	2.88	0.08	2.92	1.27	2.38(3),2.50(6),3.85(1)
$Zn@Ge_{10}^{4-}$	3.76	2.91	2.96	−0.05	2.94	1.28	2.42(3),2.53(6),3.88(1)
24 skeletal electrons							
Ge_{10}^{4-}	3.26	2.80	2.61	0.19	2.70	1.21	–
$Ni@Ge_{10}^{4-}$	3.10	3.89	2.70	1.19	3.30	0.94	2.38(3),2.42(1),2.51(3),2.55(3)
$Cu@Ge_{10}^{3-}$	3.03	3.96	2.76	1.20	3.36	0.90	2.38(4),2.53(3), 2.57(3)
$Zn@Ge_{10}^{2-}$	3.04	3.99	2.81	1.18	3.40	0.89	2.40(1),2.42(3),2.55(3),2.58(3)
22 skeletal electrons							
$Ni@Ge_{10}^{2-}$	3.26	3.13	2.67	0.46	2.90	1.12	2.32(3),2.37(3),2.40(3),3.30(1)
$Cu@Ge_{10}^{-}$	3.28	3.17	2.71	0.46	2.94	1.12	2.34(3),2.40(3),2.44(3),3.30(1)
$Zn@Ge_{10}$	3.34	3.23	2.76	0.47	3.00	1.11	2.39(3),2.43(3),2.48(3),3.34(1)
20 skeletal electrons							
Ge_{10}	2.64	2.97	2.66	0.33	2.81	0.94	–
$Ni@Ge_{10}$	3.00	3.62	2.70	0.92	3.16	0.95	2.36(3),2.41(3),2.43(3),2.46(1)
$Cu@Ge_{10}^{+}$	3.03	3.65	2.77	0.88	3.21	0.94	2.40(3),2.44(3),2.45(3),2.54(1)
$Zn@Ge_{10}^{2+}$	3.10	3.71	2.87	0.84	3.29	0.94	2.47(6),2.49(3),2.62(1)
$Ni@In_{10}^{10-}$ (exptl)[a]	≈3.3	≈4.3	≈3.2	≈1.1	≈3.75	0.88	2.8(9),2.7(1)

[a] Ref. [3].

parison of these calculated polyhedra to the experimentally found polyhedron in the $Ni@In_{10}^{10-}$ of $K_{10}In_{10}Ni$ is difficult because of deviation from C_{3v} symmetry and two independent $Ni@In_{10}^{10-}$ anions in the actual structure.[3] However, using the crude estimates in Table 3 obtained from the experimental data leads to a Δh of ≈1.1 Å and a $v/\bar{h}$ ratio of 0.88 as compared with our calculated Δh of 0.92 and $v/\bar{h}$ of 0.95 for $Ni@Ge_{10}$.

Addition of two skeletal electrons to the centered C_{3v} ten-vertex polyhedra to give structures with 22 skeletal electrons leads to significantly more elongated polyhedra as indicated by Δh values in the range 0.46–0.47 Å and $v/\bar{h}$ ratios in the range 1.11–1.12 (Table 3). Because of this elongation only nine of the ten germanium atoms are within the reasonable distances of 2.3–2.5 Å for significant direct interaction with the central metal atom. The tenth germanium atom, namely the axial germanium atom (Table 3), is now ≈3.3 Å from the central metal atom. In this case an empty C_{3v} isomer of Ge_{10}^{2-} was not found in our earlier work[21] so that a direct comparison of the effect of the central metal atom on the polyhedral geometry cannot be made.

The empty C_{3v} Ge_{10}^{4-} polyhedron with 24 skeletal electrons is rather elongated with a $v/\bar{h}$ ratio of 1.21 and a rather small Δh value of 0.19 Å. Insertion of a metal atom into the center changes the geometry drastically to bring the axial vertex even closer to the central metal atom (2.38–2.40 Å) than the other nine vertices (2.38–2.58 Å). This distortion makes three of the edges of the original tetracapped trigonal prism, namely the edges of the capped triangular face of the underlying trigonal prism, so long (≈3.9 Å as indicated directly by the h_c values in Table 3) that these distances can no longer be regarded as edges. The tetracapped trigonal prism, which is a deltahedron with 16 triangular faces, now becomes a polyhedron with 10 triangular faces and 3 quadrilateral faces.

The C_{3v} polyhedra with 26 skeletal electrons have the most elongated structures found in this work. The empty C_{3v} Ge_{10}^{6-} polyhedron[21] has the largest $v/\bar{h}$ ratio found in this work, namely 1.35, as well as a negative Δh of −0.11 Å indicating a contraction of the edges in the capped triangular face of the underlying trigonal prism. Inserting a metal atom changes the shape only to a slight extent with Δh ranging from −0.05 Å for the zinc derivative to 0.30 Å for the nickel derivative and $v/\bar{h}$ ratios in the narrow range 1.26–1.28. Only nine of the ten germanium atoms are within bonding distances of the central metal atom, namely 2.36–2.53 Å. As a consequence of the elongated structure of the 26-skeletal electron C_{3v} $M@Ge_{10}$ structures, the tenth germanium atom at the unique axial vertex is long, ≈3.8 Å from the central metal atom indicating essentially no direct interaction.

The effect of the central metal atom on the cluster molecular orbitals: The molecular orbital diagrams for the isoelectronic C_{3v} $Ni@Ge_{10}$ and $Zn@Ge_{10}^{2+}$ (**20–3**) in Figure 9 and Figure 10, respectively, depict the interactions of the bonding molecular orbitals of the empty Ge_{10} cluster with the

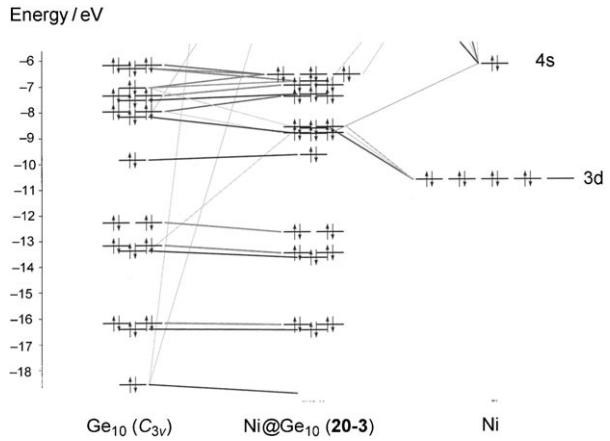

Figure 9. Molecular orbital diagram for the interaction of an interstitial nickel atom with a C_{3v} Ge_{10} cluster.

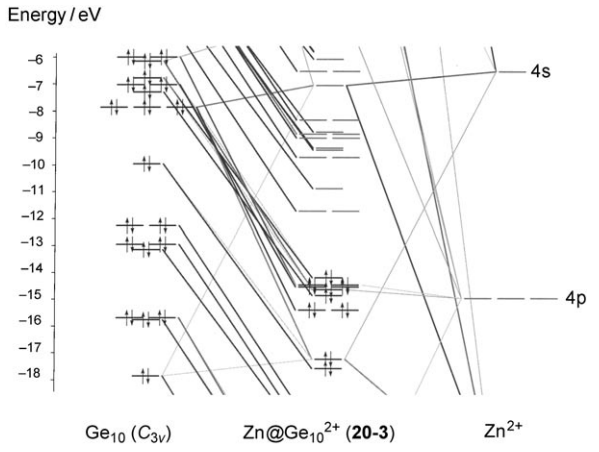

Figure 10. Molecular orbital diagram for the interaction of interstitial Zn^{2+} with a C_{3v} Ge_{10} cluster.

atomic orbitals of the interstitial metal atom. For the nickel atom in $Ni@Ge_{10}$ (**20–3(Ni)**), which is a formal zero-electron donor to the surrounding Ge_{10} cluster, there is very little interaction of the nickel atomic orbitals with the cluster molecular orbitals (Figure 9). The interstitial nickel atom thus functions as a "pseudo noble gas" with a filled $3d^{10}$ shell as has been previously discussed. [23] However, for the zinc atom in $Zn@Ge_{10}^{2+}$ (**20–3(Zn)**), which is a formal two-electron donor through ionization to Zn^{2+}, the metal interacts strongly with the cluster molecular orbitals leading to major stabilization (Figure 10). A similar pattern of interaction of the central metal atoms is observed in the corresponding $M@Ge_{10}$ clusters of four-fold symmetry (**20–4**).

Summary

Structures with three-fold, four-fold, and five-fold symmetry are found by DFT for centered 10-vertex bare germanium clusters of the general type $M@Ge_{10}^{z}$ depending on the central metal atom M and the skeletal electron count. Thus for $M@Ge_{10}$ clusters with 20 skeletal electrons the DFT results are consistent with experimental data on isoelectronic centered 10-vertex bare metal clusters. The lowest energy structure for $Ni@Ge_{10}$, isoelectronic with the known $Ni@In_{10}^{10-}$ in $K_{10}In_{10}Ni$,[3] is a C_{3v} polyhedron derived from the tetracapped trigonal prism. However, for $Zn@Ge_{10}^{2+}$, isoelectronic with the known $Zn@In_{10}^{8-}$ in $K_8In_{10}Zn$,[4] the lowest energy structure is a D_{4d} bicapped square antiprism. For the clusters $Ni@Ge_{10}^{2-}$, $Cu@Ge_{10}^{-}$, and $Zn@Ge_{10}$ with 22 skeletal electrons the lowest energy structures are found to be the D_{4d} bicapped square antiprism predicted by the Wade–Mingos rules.[15,16,17,18] For the clusters $Ni@Ge_{10}^{4-}$, $Cu@Ge_{10}^{3-}$, and $Zn@Ge_{10}^{2-}$ with 24 skeletal electrons the lowest energy structures are C_{3v} polyhedra with 10 triangular faces and 3 quadrilateral faces derived from a tetracapped trigonal prism by extreme lengthening of the edges of the capped face of the underlying trigonal prism. For the clusters $Cu@Ge_{10}^{5-}$ and $Zn@Ge_{10}^{4-}$ with 26 skeletal electrons the lowest energy structures are the D_{5d} pentagonal antiprism predicted by the Wade–Mingos rules[15,16,17,18] with the C_{3v} tetracapped trigonal prism as a somewhat higher energy structure. However, for the isoelectronic $Ni@Ge_{10}^{6-}$ the relative energies of these two structures are reversed so that the C_{3v} tetracapped trigonal prism becomes the global minimum.

Acknowledgements

We are indebted to the National Science Foundation for partial support of this work under Grants CHE-0209857 and CHE-0716718. Part of this work was undertaken with the financial support from the Romanian CEEX-42 SUPRAMOL program.

[1] J. D. Corbett, *Struct. Bonding* (Berlin) **1997**, *87*, 157.
[2] J. D. Corbett, *Angew. Chem.* **2000**, *112*, 682; *Angew. Chem. Int. Ed.* **2000**, *39*, 670.
[3] R. W. Henning, J. D. Corbett, *Inorg. Chem.* **1999**, *38*, 3883.
[4] S. C. Sevov, J. C. Corbett, *Inorg. Chem.* **1993**, *32*, 1059.
[5] M. Ruck, V. Dubenskyy, T. Söhnel, *Angew. Chem.* **2000**, *115*, 3027; *Angew. Chem. Int. Ed.*, **2003**, *45*, 2978.
[6] A. Spiekermann, S. D. Hoffmann, T. F. Fässler, *Angew. Chem.* **2006**, *118*, 3538; *Angew. Chem. Int. Ed.* **2006**, *45*, 3459.
[7] E. N. Esenturk, J. Fettinger, B. Eichhorn, *Chem. Commun.* **2005**, 247.
[8] S. H. Vosko, L. Wilk, M. Nusair, *Can. J. Phys.* **1980**, *58*, 1200.
[9] C. Lee, W. Yang, R. G. Parr, *Phys. Rev. B* **1988**, *37*, 785.
[10] A. D. Becke, *J. Chem. Phys.* **1993**, *98*, 5648.
[11] P. J. Stephens, F. J. Devlin, C. F. Chabalowski, M. J. Frisch, *J. Phys. Chem.* **1994**, *98*, 11623.
[12] Gaussian 98, Revision A.11.3, M. J. Frisch, G. W. Trucks, H. B. Schlegel, G. E. Scuseria, M. A. Robb, J. R. Cheeseman, V. G. Zakrzewski, J. A. Montgomery, Jr., R. E. Stratmann, J. C. Burant, S. Dapprich, J. M. Millam, A. D. Daniels, K. N. Kudin, M. C. Strain, O. Farkas, J. Tomasi, V. Barone, M. Cossi, R. Cammi, B. Mennucci, C. Pomelli, C. Adamo, S. Clifford, J. Ochterski, G. A. Petersson, P. Y. Ayala, Q. Cui, K. Morokuma, D. K. Malick, A. D. Rabuck, K. Raghavachari, J. B. Foresman, J. Cioslowski, J. V. Ortiz, A. G. Baboul, B. B. Stefanov, G. Lui, A. Liashenko, P. Piskorz, I. Komaromi, R. Gomperts, R. L. Martin, D. J. Fox, T. Keith, M. A. Al-Laham, C. Y. Peng, A. Nanayakkara, C. Gonzalez, M. Challacombe, P. M. W. Gill, B. G.

Johnson, W. Chen, M. W. Wong, J. L. Andres, M. Head-Gordon, E. S. Replogle, J. A. Pople, Gaussian, Inc., Pittsburgh, PA, **2002**.
[13] Y. Xie, H. F. Schaefer III; R. B. King, *J. Am. Chem. Soc.* **2000**, *122*, 8746.
[14] Scientific Computing and Modeling NV, Vrije Universiteit, Theoretical Chemistry, De Boelelaan 1083, 1081 HV Amsterdam, The Netherlands.
[15] K. Wade, *J. Chem. Soc. D* **1971**, 792.
[16] K. Wade, *Adv. Inorg. Chem. Radiochem.* **1976**, *18*, 1.
[17] D. M. P. Mingos, *Nature Phys. Sci.* **1972**, *99*, 236.
[18] D. M. P. Mingos, *Accts. Chem. Res.* **1984**, *17*, 311.
[19] E. L. Muetterties, *Boron Hydride Chemistry*, Academic Press, New York, **1975**.
[20] W. N. Lipscomb, R. J. Wiersema, M. F. Hawsthorne, *Inorg. Chem.* **1972**, *11*, 651.
[21] R. B. King, I. Silaghi-Dumitrescu, M. M. Uţă, *Inorg. Chem.* **2006**, *45*, 4974.
[22] G. Ciani, A. Sironi, S. Martinengo, L. Garlaschelli, R. Della Pergola, P. Zanello, F. Laschi, N. Masciocchi, *Inorg. Chem.* **2001**, *40*, 3905.
[23] R. B. King, *Dalton Trans.* **2004**, 3420.

Received: October 7, 2007
Published online: April 2, 2008

